Supporting Information:

Mixed excitonic nature in water-oxidized $BiVO_4$ surfaces with defects

Rachel Steinitz-Eliyahu,[1] Daniel Hernangómez-Pérez,[1] Franziska S. Hegner,[2] Pavle Nikačević,[2] Núria López,[2] and Sivan Refaely-Abramson[1]

[1]*Department of Molecular Chemistry and Materials Science, Weizmann Institute of Science, Rehovot 7610001, Israel*

[2]*Institut Català d'Investigació Química (ICIQ), The Barcelona Institute of Science and Technology (BIST), Avda. Països Catalans, 16, 43007 Tarragona, Spain.*

CONTENTS

I. COMPUTATIONAL DETAILS

We used density functional theory (DFT) to compute the electronic structure and starting-point wavefunctions of the four structures analyzed in this manuscript. These structures were optimized in Ref. [1] employing the PBESol functional. In each case, we use a supercell containing six $BiVO_4$ layers along the $\hat{c}$ direction with 14 Å of vacuum distance. Each supercell is composed of about $150-160$ atoms (see Fig. I for an example of the supercell). All DFT calculations were done using the DFT implementation from the QUANTUM ESPRESSO package [2]. As exchange correlation potential we considered the semilocal Perdew–Burke–Ernzerhof (PBE) exchange-correlation functional [3]. This functional has been shown provide results closer to experiment for the bulk monoclinic phase of $BiVO_4$ compared to hybrid functionals (see Ref. [4] and references therein). We employed a plane-wave basis set with an energy cut-off of 90 Ry, and include spin-orbit coupling (SOC) through fully relativistic norm-conserving pseudopotentials [5]. We sampled reciprocal space with a uniform $2\times2\times1$ **k**-point grid.

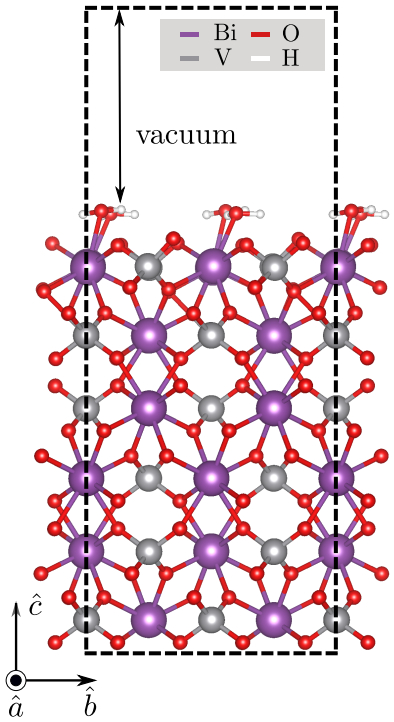

Fig. S1. Example geometry of the $BiVO_4$ supercell for the pristine structure (violet: Bi, grey: V, red: O, white: H). (a) Side view of the pristine supercell [$\hat{a} = (100)$, $\hat{b} = (010)$, $\hat{c} = (001)$]. The dashed lines denote the supercell limits.

Using DFT as a starting point, we applied many-body perturbation theory implemented in the BerkeleyGW package [6] and computed self-energy corrections within a one-shot G_0W_0 approximation. We employed the Hybertsen-Louie generalized plasmon-pole model for the frequency dependence of the dielectric screening [7]. We considered a 30 Ry screening energy cut-off and

a total of 3500 electronic bands, among them 1280 occupied. For optical absorption spectra and excitonic properties, we solved the Bethe-Salpether equation within the Tamm-Dancoff approximation [8]. For the kernel and absorption calculations we considered 14 valence (occupied) bands and 16 conduction (empty) bands. The electron-hole coupling and the optical excitations were quantified following the methods described in Sec. V.

II. BAND STRUCTURES

In Fig. S2, we show the DFT-computed band structures of the four surface structures studied in this work. We observe that the valence and conduction bands, as well as the oxo bands, all present a relatively small dispersion thus allowing us to focus our attention on the direct band-gap and energy levels at the Γ point in the main paper.

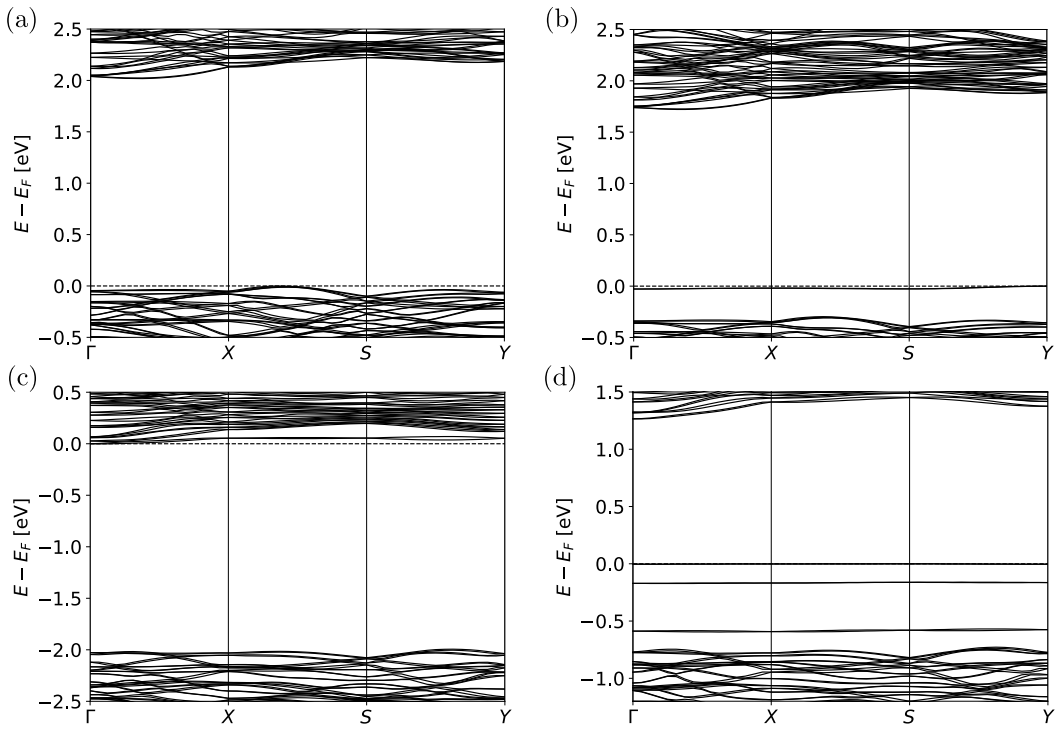

Fig. S2. Band structures of the (a) pristine, (b) pristine-peroxo, (c) split vacancy and (d) split-vacancy-oxo systems obtained using density functional theory. The band energies are normalized to the Fermi energy, defined as the highest occupied level in each system and computed along a squared path in the two-dimensional Brillouin zone.

III. ABSOLUTE DEFECT STATE ALIGNMENT

The energies in Fig. 2 of the main text are referred to the highest occupied state at the Gamma point that does not have defect character. This state has the same nature in the four systems considered in our manuscript, therefore, allowing to easily make cross-comparisons between the different systems.

We can also refer the energies with respect to the vacuum level to compare the absolute alignment of the defect levels in the DFT and GW calculations. Table I below summarizes the shift of the defect/oxo states from the DFT to the GW calculation. It is interesting to note that while for the pristine oxo system the impact of the many-body interactions that are accounted for in GW is small, for the defect systems many-body effects can produce large shift in the localized states. The large shifts, together with the associated mixed nature of the states that they may induce points to the importance of performing many-body perturbation theory at the GW level in order to study the excited state properties in these systems since they cannot be deduced by operating at the DFT level only.

System	State	$E_{\mathrm{GW}} - E_{\mathrm{DFT}}$ [eV]
Pristine-peroxo	oxo	0.041
Split-vacancy	d1	1.357
	d2	1.376
Split-vacancy-oxo	oxo1	-0.481
	oxo2	-0.413
	oxo3	-0.374

TABLE I. Absolute alignment between GW and DFT of the defect/oxo states.

IV. OVERLAP MATRIX ELEMENTS

The calculation of the overlap matrix elements at the Γ point mentioned in the main text is performed by averaging over blocks of degenerate spin states according to

$$S_{AB} = \frac{1}{4} \sum_{\sigma_1,\sigma_2} \left| \left\langle \phi_A^{\sigma_1,\sigma_2} \middle| \phi_B^{\sigma_1,\sigma_2} \right\rangle \right|^2, \tag{1}$$

where A and B are two different systems, σ_1 and σ_2 are two spin projections. We also account for numerical uncertainties (random phases in the states coming from numerical diagonalization of the Kohn-Sham Hamiltonian) by averaging over a certain small number of configurations.

For completeness with the main text, we compare the overlap matrix elements of the non-oxidized and oxidized structures with the overlap of the defect and non-defect structures in Fig. S3). Surprisingly, we find that compared to the overlap elements in the main text, they vanish almost completely when comparing between the pristine and the split vacancy structures, for both water and oxo adsorbates, Fig. S3c and Fig. S3d. In both cases, the presence of defects considerably changes the structure and hence the charge distribution associated with it. In other words, the defect states cannot be considered merely as additional surface states to the pristine system; instead, they rather change the atomic structure and the associated electronic nature.

V. EXCITON COMPONENTS

As explained in Sec. I, the exciton states were obtained from the solution of the Bethe-Salpether equation [8]

$$(E_c - E_v) A^S_{vc\mathbf{k}} + \sum_{\mathbf{k}'v'c'} K_{vc\mathbf{k};v'c'\mathbf{k}'}(\Omega_c) A^S_{v'c'\mathbf{k}'} = \Omega_c A^S_{vc\mathbf{k}}, \tag{2}$$

where E_c, E_v are the conduction and valence band energies, $K_{v,c,\mathbf{k},v',c',\mathbf{k}'}$ the electron-hole interaction kernel. This is a generalized eigenvalue problem whose solution yields the exciton energies, Ω_c, and exciton coefficients, $A^S_{v,c,\mathbf{k}}$ labeled by the index S and the quantum numbers $v, c, \mathbf{k}$. These coefficients correspond to the expansion coefficients of the exciton states, Ψ^S, as linear combination direct products of single-particle electron, $\psi_{c\mathbf{k}}(\mathbf{r}_e)$, and hole, $\psi_{v\mathbf{k}}(\mathbf{r}_h)$, states

$$\Psi^S(\mathbf{r}_e, \mathbf{r}_h) = \sum_{\mathbf{k}vc} A^S_{vc\mathbf{k}} \psi_{c\mathbf{k}}(\mathbf{r}_e) \psi^*_{v\mathbf{k}}(\mathbf{r}_h). \tag{3}$$

As mentioned in the main text, the contribution of a given occupied band, v (resp. empty, c) is computed by summing $|A^S_{vc\mathbf{k}}|^2$ over $\mathbf{k}$ and c quantum numbers (resp. $\mathbf{k}$ and v) and weighting the result by the corresponding oscillator strength (see also Ref. [9]).

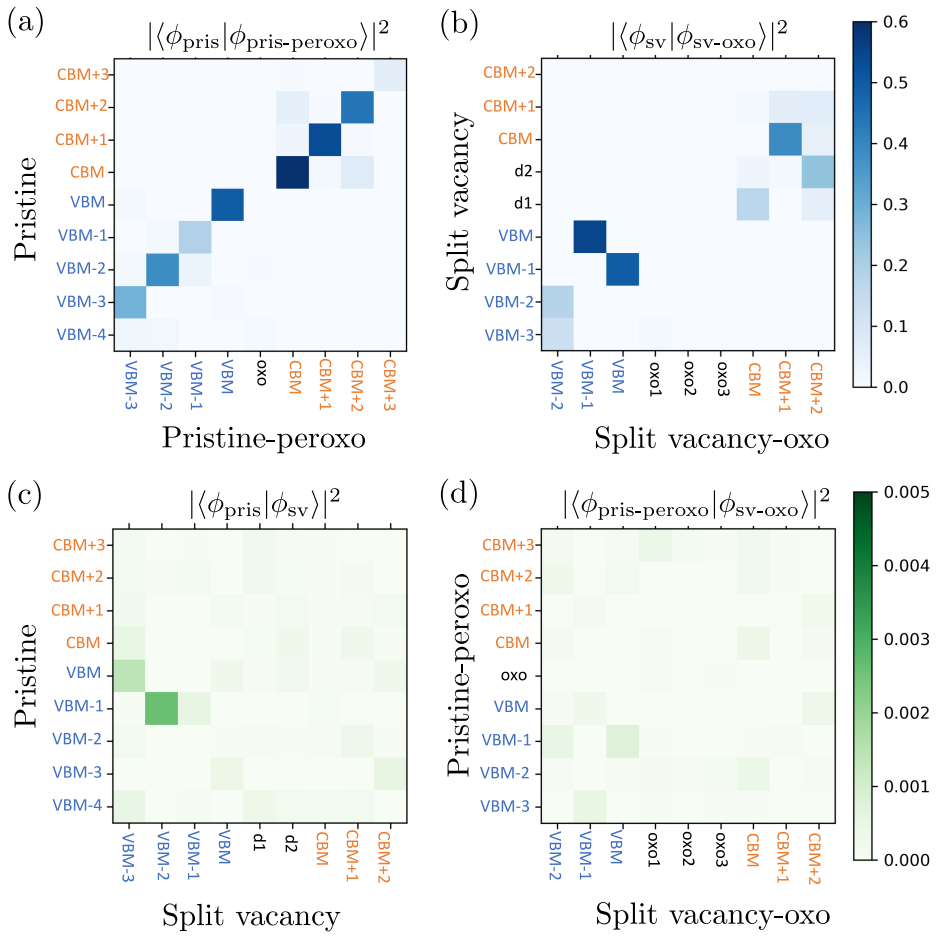

Fig. S3. Overlap matrix elements $S_{AB} = |\langle\phi_A|\phi_B\rangle|^2$ for selected states of pristine and pristine-peroxo systems. The scale ranges from 0 to 1, 0 being no overlap and 1 being complete overlap (same wavefunction up to a phase factor). (b) Same as in (a) but for split vacancy and split vacancy-oxo, (c) pristine and split vacancy and (d) pristine-peroxo and split vacancy-oxo overlap matrix elements. Note that the scale in the two upper panels is two orders of magnitude larger than in the two lower panels.

VI. ADDITIONAL ABSORPTION DATA

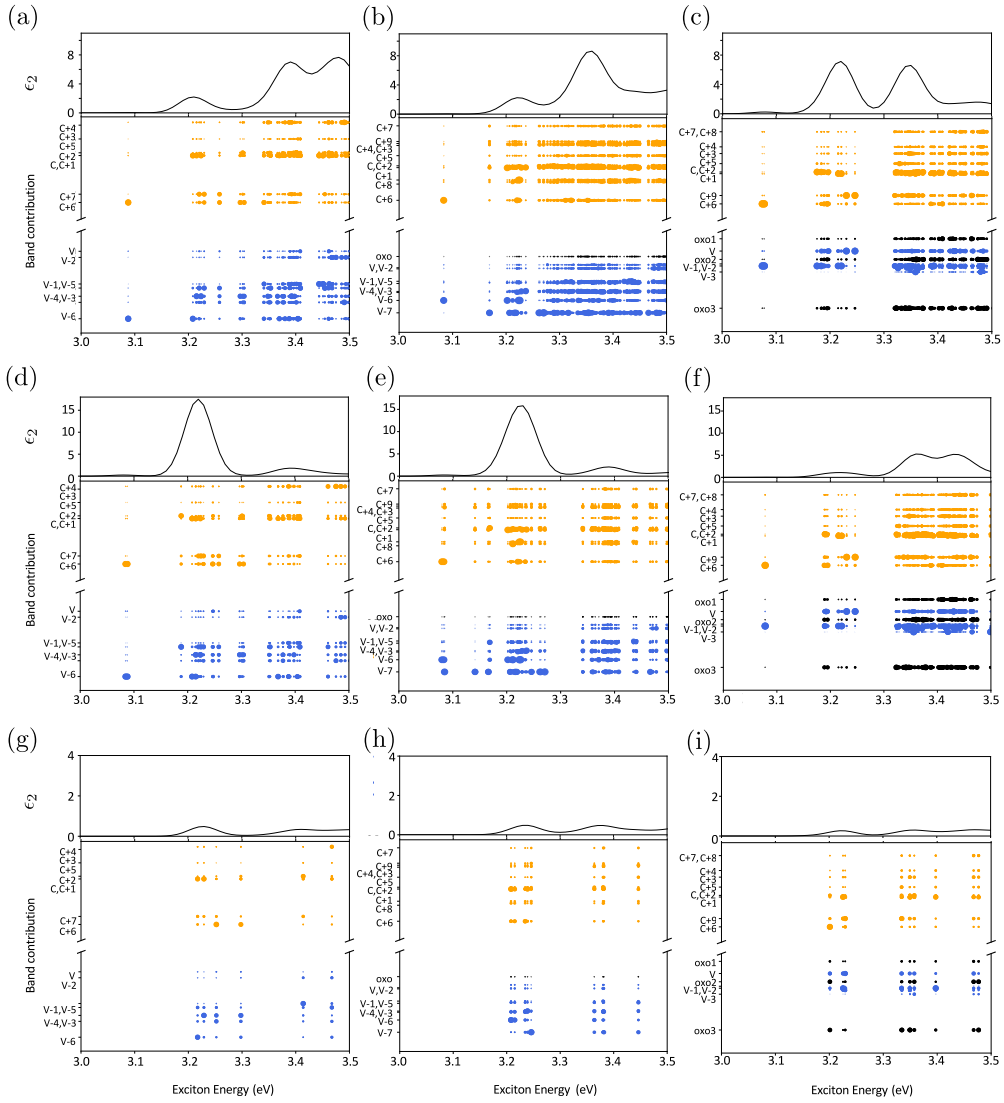

Fig. S4. Absorption spectra (in arbitrary units) and contribution from each valence (blue), oxo (black) and conduction bands (orange) to the exciton states (given by adding all circles at a given energy). The size of the circle is obtained following Sec. V. (a)-(c) pristine, pristine-peroxo and split-vacancy-oxo structures with absorption occurring for the $\hat{a} = (100)$ polarization direction; (d)-(f) pristine, pristine-peroxo and split-vacancy-oxo structures with absorption occurring for the $\hat{b} = (010)$ polarization direction and (g)-(i) pristine, pristine-peroxo and split-vacancy-oxo structures with absorption occurring for the $\hat{c} = (001)$ polarization direction. The order of the levels correspond to the GW ordering of energy states.

[1] P. Nikacčvić, F. S. Hegner, J. R. Galán-Mascarós, and N. López, Influence of oxygen vacancies and surface facets on water oxidation selectivity toward oxygen or hydrogen peroxide with $BiVO_4$, ACS Catalysis **11**, 13416 (2021).

[2] Giannozzi et al., Journal of Physics: Condensed Matter **21**, 395502 (2009).

[3] J. P. Perdew, K. Burke, and M. Ernzerhof, Generalized gradient approximation made simple, Physical Review Letters **77**, 3865 (1996).

[4] J. Wiktor, I. Reshetnyak, F. Ambrosio, and A. Pasquarello, Comprehensive modeling of the band gap and absorption spectrum of $BiVO_4$, Physical Review Materials **1**, 022401 (2017).

[5] D. Hamann, Optimized norm-conserving vanderbilt pseudopotentials, Physical Review B **88**, 085117 (2013).

[6] J. Deslippe, G. Samsonidze, D. A. Strubbe, M. Jain, M. L. Cohen, and S. G. Louie, BerkeleyGW: A massively parallel computer package for the calculation of the quasiparticle and optical properties of materials and nanostructures, Computer Physics Communications **183**, 1269 (2012).

[7] M. S. Hybertsen and S. G. Louie, Electron correlation in semiconductors and insulators: Band gaps and quasiparticle energies, Physical Review B **34**, 5390 (1986).

[8] M. Rohlfing and S. G. Louie, Electron-hole excitations in semiconductors and insulators, Physical Review Letters **81**, 2312 (1998); Electron-hole excitations and optical spectra from first principles, Physical Review B **62**, 4927 (2000).

[9] S. Refaely-Abramson, D. Y. Qiu, S. G. Louie, and J. B. Neaton, Defect-induced modification of low-lying excitons and valley selectivity in monolayer transition metal dichalcogenides, Physical Review Letters **121**, 167402 (2018).